arXiv:1008.4191v2 [cond-mat.supr-con] 27 Mar 2011

Monte Carlo study of thermal fluctuations and Fermi-arc formation in d-wave superconductors

Yong-Wei Zhong,[1,2] Tao Li,[1] and Qiang Han[1,3]

[1]*Department of Physics, Renmin University, Beijing, China*
[2]*Tongji Zhejiang College, Jiaxing, Zhejiang, China*
[3]*Department of Physics and Center of Theoretical and Computational Physics, The University of Hong Kong, Pokfulam Road, Hong Kong, China*

(Dated: March 29, 2011)

From the perspective of thermal fluctuations, we investigate the pseudogap phenomena in underdoped high-temperature curpate superconductors. We present a local update Monte Carlo procedure based on the Green's function method to sample the fluctuating pairing field. The Chebyshev polynomial method is applied to calculate the single-particle spectral function directly and efficiently. The evolution of Fermi arcs as a function of temperature is studied by examining the spectral function at Fermi energy as well as the loss of spectral weight. Our results signify the importance of the vortex-like phase fluctuation on the formation of Fermi arcs.

PACS numbers: 74.72.-h, 74.20.Rp, 74.25.Jb

I. INTRODUCTION

The mysterious pseudogap (PG) phase is one of the most fascinating aspects of the underdoped high-temperature curpate superconductors (HTCS). By a variety of probes the pseudogap (the suppression of the low-energy single-particle spectral weight) has been observed to persist from above the superconducting (SC) critical temperature T_c to T^* in the underdoped regime. The direct evidences of this spectral gap come from the angle-resolved photoemission spectroscopy (ARPES) [1–3]. Ding *et al.*[1] studied the underdoped $Bi_2Sr_2CaCu_2O_{8+\delta}$ using ARPES and found that a pseudogap with d-wave symmetry begins to open up for $T < T^*$ and develops smoothly into the d-wave SC gap below T_c. One peculiar property of the pseudogap phase revealed by further experimental investigation is the truncated Fermi surface termed as Fermi arcs,[4] exhibiting distinct difference from the point-like (four gap nodes) Fermi surface for T well below T_c as expected for a pure d-wave superconductor and the closed Fermi surface for T above T^*.

There are two basic scenarios of the PG phase. The first one attributes the opening of the pseudogap to the presence of an exotic order competing with the SC phase, such as the spin[5,6] and/or charge[7] density waves and so on. The second scenario associates the PG phase with the phase-incoherent pairing and therefore the pseudogap is interpreted as a precursor of the SC order. In this preformed-pair scenario there are two energy scales: one is the BCS energy gap Δ which is closely related to the binding energy of the electron pair, and the other is the phase-stiffness energy scale T_θ which protects the phase coherence. For the conventional superconductors T_θ is larger than Δ so that the SC state is destroyed by pair breaking. However for the underdoped HTCS, because of the low carrier density and the short correlation length, Δ is larger than T_θ,[8] and therefore the phase coherence is destroyed while the energy gap survives as temperature increases across T_c. In this context T_c is determined by T_θ and the pseudogap is caused by the pair fluctuations[8–18]. Franz and Millis[13] showed that random supercurrent induced by thermal phase fluctuations can cause the shift of electronic spectral weight in both momentum and energy. Berg and Altman[14] further attributed the emergence of the Fermi arc to the pile up of the low-energy spectral weight along the underlying Fermi surface due to the Doppler-shift effect of the fluctuating supercurrent. This picture of phase fluctuations is concise and instructive, yet the analytical results relied on the semiclassical approximation[13] where only far-field effect of the vortex-type excitations is considered, which might be uncontrolled as argued in Ref.[16]. Furthermore, the probability distribution of the fluctuating supercurrent was assumed phenomenologically to be Gaussian type. Recently we[17,18] attempted to go beyond the semiclassical approximation by employing a 2D XY model to simulate the vortex-type phase fluctuations and numerically taking both the Doppler effect of the whirling supercurrent and the scattering effect of vortices as topological singularities into full consideration. However, the XY model is still a phenomenological description of the phase fluctuations, which includes a temperature-independent phase-stiffness constant J.

In this work, we start from a 2D attractive Hubbard model with only nearest-neighbor interactions to investigate the pseudogap phase and the evolution of Fermi arcs in d-wave superconductors. The path-integral formalism is employed where pairing fluctuations are inherently embedded. A local-update Monte Carlo scheme on the basis of the Green's function method is presented to speed up the random walk in the classical configuration space of pairing field. Superfluid density is calculated as the signature of the SC phase transition and compared with the phase correlation function[12]. The single-electron spectral function is calculated using Chebyshev polynomial method[17–20]. The temperature dependence of Fermi-arc length is discussed.

The paper is organized as follows: In Section II we describe the basic path-integral formalism to treat the 2D extended Hubbard model. The local-update algorithm based on Green's function theory and the Chebyshev expansion approach are presented. In Section III, we calculate the temperature dependencies of various quantities relevant to the phase fluctuations and pseudogap phase. The conclusion is given in Section IV.

II. THE MODEL AND FORMALISM

The BCS Hamiltonian $\hat{H}_{\rm BCS}$ we adopt is given by:

$$\begin{aligned}\hat{H}_{\rm BCS} &= -t\sum_{i,\delta,\sigma} c^\dagger_{i\sigma}c_{i+\delta\sigma} - t'\sum_{i,\delta',\sigma} c^\dagger_{i\sigma}c_{i+\delta'\sigma} \\ &\quad -V\sum_{i,\delta} c^\dagger_{i\uparrow}c_{i\uparrow}c^\dagger_{i+\delta\downarrow}c_{i+\delta\downarrow} - \mu\sum_{i,\sigma} n_{i,\sigma}. \quad (1)\end{aligned}$$

Here σ denotes spin. i is the index of site of the two-dimensional $L\times L$ square lattice. $i+\delta$ and $i+\delta'$ denote the nearest-neighboring (NN) and next-NN sites of i, respectively. t and t' are the NN and next-NN hopping integrals, respectively. μ is the chemical potential. The attractive interaction $V>0$ between electrons on the NN sites favors unconventional superconducting phases. To investigate the effect of superconducting fluctuations, the quantum partition function is expressed in the path integral formalism [21,22]:

$$Z = \int D\{\varphi_{i\sigma}(\tau),\bar{\varphi}_{i\sigma}(\tau)\}\exp(-S) \quad (2)$$

where the action S is expressed as

$$S(\varphi,\bar{\varphi}) = \int_0^\beta d\tau\left[\sum_{i\sigma}\bar{\varphi}_{i\sigma}(\tau)(\partial_\tau-\mu)\varphi_{i\sigma}(\tau) - \sum_{i,j,\sigma} t_{ij}\bar{\varphi}_{i\sigma}(\tau)\varphi_{j\sigma}(\tau) - V\sum_{i,\delta}\bar{\varphi}_{i\uparrow}(\tau)\bar{\varphi}_{i+\delta\downarrow}(\tau)\varphi_{i+\delta\downarrow}(\tau)\varphi_{i\uparrow}(\tau)\right], \quad (3)$$

where $\varphi_{i\sigma}$ and $\bar{\varphi}_{i\sigma}$ denote Grassmann fields and $\beta = 1/k_BT$. We then decouple the quartic term in the action by introducing an auxiliary Hubbard-Stratonovich field $\Delta_{i,i+\delta}(\tau)$ in the Cooper channel. For a square lattice with N sites and periodic boundary condition, there are totally $2N(N=L^2)$ independent $\Delta_{i,i+\delta}(\tau)$'s. Hereafter we use Δ to denote the set $\{\Delta_{i,i+\delta}(\tau)\}$. The partition function now becomes

$$Z = \int D\Delta D\bar{\Delta} e^{-\beta\Omega(\Delta,\bar{\Delta})}, \quad (4)$$

where

$$\int D\Delta D\bar{\Delta} \equiv \int\prod_{i=1}^{N}\prod_{\delta=\hat{x},\hat{y}} d\Delta_{i,i+\delta}(\tau)d\bar{\Delta}_{i,i+\delta}(\tau). \quad (5)$$

In Eq. (4), the grand potential is expressed as

$$\Omega(\Delta,\bar{\Delta}) = \Omega_f(\Delta,\bar{\Delta}) + V^{-1}\sum_{i,\delta}|\Delta_{i,i+\delta}(\tau)|^2, \quad (6)$$

where Ω_f denotes the fermionic thermodynamic potential

$$\Omega_f(\Delta,\bar{\Delta}) = -\beta^{-1}\ln{\rm Tr}e^{-\beta\hat{H}_{\rm BdG}(\Delta)}. \quad (7)$$

Here the BdG Hamiltonian is written by

$$\begin{aligned}\hat{H}_{\rm BdG}(\Delta) &= \Psi^\dagger\tilde{H}_{\rm BdG}(\Delta)\Psi \quad (8)\\ &= \sum_{i,j=1}^{N}(c^\dagger_{i\uparrow}, c_{i\downarrow})\begin{pmatrix}-t_{i,j} & \Delta_{i,j}\\ \Delta^*_{i,j} & t_{i,j}\end{pmatrix}\begin{pmatrix}c_{j\uparrow}\\ c^\dagger_{j\downarrow}\end{pmatrix}\end{aligned}$$

where $\Psi^\dagger(\Psi)$ denotes the Nambu creation (annihilation) operator defined as $\Psi^\dagger = (c^\dagger_{1\uparrow}, c_{1\downarrow}, c^\dagger_{2\uparrow}, c_{2\downarrow}, \cdots, c^\dagger_{N\uparrow}, c_{N\downarrow})$. $\tilde{H}_{\rm BdG}$ is a $2N\times 2N$ Hermitian matrix which will be called BdG matrix. Hereafter we use capital letters with a tilde ($\tilde{}$) to denote $2N\times 2N$ dimensional matrices (e.g. the BdG matrix $\tilde{H}_{\rm BdG}$) while a hat ($\hat{}$) to denote operators in second quantization (e.g. the BdG Hamiltonian $\hat{H}_{\rm BdG}$). For the sake of convenience, we will omit the argument Δ and simply use $\hat{H}_{\rm BdG}$ and $\tilde{H}_{\rm BdG}$ to denote the BdG Hamiltonian and matrix for a certain pairing field Δ.

In the following, we will ignore the τ-dependence of $\Delta_{i,i+\delta}(\tau)$, i.e. the quantum fluctuation, and concentrate on its thermal fluctuations expected to be dominant near T_c especially in the high temperature pseudogap region. With this approximation, $\hat{H}_{\rm BdG}$ actually describes the electrons moving in a static but spatially fluctuating pairing field. Moreover Eq. (4) becomes a classical partition function expressed as an integration over the classical phase space formed by $\{\Delta_{i,i+\delta} = |\Delta_{i,i+\delta}|e^{i\phi^\delta_i}\}$, whose dimension is $4N$ for a N-site square lattice. Such multidimensional integration can be performed by the standard Monte Carlo method. To achieve this goal, one need to obtain the probability distribution $P(\Delta)\propto e^{-\beta\Omega(\Delta,\bar{\Delta})}$ for a configuration Δ, or its change characterized by the ratio

$$\frac{P(\Delta')}{P(\Delta)} = e^{-\beta[\Omega(\Delta',\bar{\Delta}')-\Omega(\Delta,\bar{\Delta})]}, \quad (9)$$

for a possible change of configuration $\Delta \to \Delta'$. The acceptance probability for such a change is given by

$$P_{\rm A}(\Delta' \leftarrow \Delta) = \min\left[1, \frac{P(\Delta')}{P(\Delta)}\right] \tag{10}$$

according to the Metropolis algorithm. To obtain Ω especially the nontrivial Ω_f, previous numerical work[12] related it to the eigen-spectrum of the BdG matrix through the relation $\Omega_f(\Delta, \bar{\Delta}) = -\beta^{-1}\sum_n \ln(1+e^{-\beta\epsilon_n})$, where ϵ_n is the eigenvalue of the BdG equations,

$$\sum_j \begin{pmatrix} -t_{ij} & \Delta_{i,j} \\ \Delta^*_{i,j} & t^*_{i,j} \end{pmatrix} \begin{pmatrix} u^j_n \\ v^j_n \end{pmatrix} = \epsilon_n \begin{pmatrix} u^i_n \\ v^i_n \end{pmatrix} \tag{11}$$

To solve this eigenvalue problem, one needs to diagonalize a $2N\times 2N$ BdG matrix and the workload is $O(N^3)$ which is quite time-consuming for large lattice.

In this paper, we will propose an alternative local-update scheme based on the Green's function method. The Gor'kov Green's function is employed, which is defined as:

$$G(i\tau, j\tau') = -{\rm T}\left\langle \begin{array}{cc} c_{i\uparrow}(\tau)c^\dagger_{j\uparrow}(\tau') & c_{i\uparrow}(\tau)c_{j\downarrow}(\tau') \\ c^\dagger_{i\downarrow}(\tau)c^\dagger_{j\uparrow}(\tau') & c^\dagger_{i\downarrow}(\tau)c_{j\downarrow}(\tau') \end{array} \right\rangle, \tag{12}$$

in terms of 2×2 Nambu matrix notation. Here $\langle\cdots\rangle = {\rm Tr}[\cdots e^{-\beta\tilde{H}_{\rm BdG}}]/{\rm Tr}[e^{-\beta\tilde{H}_{\rm BdG}}]$, and its Fourier transform with respect to the imaginary time is

$$G(i,j;i\omega_k) = \int_0^\beta d\tau G(i\tau, j0)e^{i\omega_k\tau} \tag{13}$$

where $\omega_k = 2\pi T(k+1)$ the Matsubara frequencies. One can easily find that the matrix form of the Gor'kov Green's function is actually the resolvent of the BdG matrix $\tilde{H}_{\rm BdG}$, i.e.

$$\tilde{G}(i\omega_k) = (i\omega_k\tilde{I} - \tilde{H}_{\rm BdG})^{-1}, \tag{14}$$

where $\tilde{I}$ the unity matrix. Combining this relation with Eq. (11), we obtain the spectral representation of $\tilde{G}(i\omega_k)$,

$$G(i,j;i\omega_k) = \sum_{\epsilon_n} \frac{\begin{pmatrix} u^i_n \\ v^i_n \end{pmatrix}(u^j_n, v^j_n)^*}{i\omega_k - \epsilon_n} \tag{15}$$

which is a 2×2 matrix. Before starting our simulation, we only need to diagonalize the BdG matrix with certain initial (often random) configuration once for all. Then the eigen-energies ϵ_n and eigen-functions u_n and v_n are used to calculate the Green's function according to Eq. (15). As we will show in Section II A, we can always update the Gor'kov Green's function without having to diagonalize the BdG matrix any more as long as the change of configuration is proposed locally.

A. Update of the Green's function and calculation of the acceptance probability

We assume a local change of the configuration, located at the 1 and 2 sites without loss of generality, from $\Delta_{1,2}$ to $\Delta'_{1,2} = \Delta_{1,2} + \chi_{1,2}$. Then the BdG Hamiltonian becomes

$$\hat{H}'_{\rm BdG} = \hat{H}_{\rm BdG} + \hat{H}_1 \tag{16}$$

$$\hat{H}_1 = \chi_{1,2}(c^\dagger_{1\uparrow}c^\dagger_{2\downarrow} + c^\dagger_{2\uparrow}c^\dagger_{1\downarrow}) + h.c. \tag{17}$$

where $\hat{H}_1$ denotes the corresponding change of the BdG Hamiltonian. According to Eq. (14), we have

$$\begin{aligned} \tilde{G}'(i\omega_n) &= (i\omega_k\tilde{I} - \tilde{H}_{\rm BdG} - \tilde{H}_1)^{-1} \\ &= \tilde{G}(i\omega_n)[1 - \tilde{H}_1\tilde{G}(i\omega_n)]^{-1}, \end{aligned} \tag{18}$$

where $\tilde{H}_1$ denotes the matrix form of $\hat{H}_1$ in the Nambu representation as Eq.(8),

$$\tilde{H}_1 = \left(\begin{array}{c|c} X_{4\times 4} & 0 \\ \hline 0 & 0 \end{array}\right)_{2N\times 2N} \tag{19}$$

where only its upper-left-corner 4×4 block is has non-zero elements, and $X_{4\times 4}$ is

$$X_{4\times 4} = \begin{pmatrix} 0 & 0 & 0 & \chi_{1,2} \\ 0 & 0 & \chi^*_{1,2} & 0 \\ 0 & \chi_{1,2} & 0 & 0 \\ \chi^*_{1,2} & 0 & 0 & 0 \end{pmatrix}. \tag{20}$$

The inverse operation on the right hand of Eq. (18) can be performed as follows,

$$(I - \tilde{H}_1\tilde{G})^{-1} = \left[I - \begin{pmatrix} X & 0 \\ 0 & 0 \end{pmatrix}\begin{pmatrix} A & B \\ C & D \end{pmatrix}\right]^{-1} \tag{21}$$

$$= \begin{pmatrix} I - XA & -XB \\ 0 & I \end{pmatrix}^{-1} \tag{22}$$

$$= \begin{bmatrix} (I-XA)^{-1} & (I-XA)^{-1}XB \\ 0 & I \end{bmatrix}. \tag{23}$$

In the above derivation, we use block matrices A, B, C, D to denote $\tilde{G}$, whose dimension is 4×4, $4\times(2N-4)$, $(2N-4)\times 4$ and $(2N-4)\times(2N-4)$, respectively. As most non-zero elements of the above matrix is concentrated on the first four rows, one can update $\tilde{G}'$ according to Eq. (18) with $O(N^2)$ computing operations.

Next, we will shown how to obtain the change of the thermodynamic potential which determines the acceptance of the proposed local update. According to textbook[23], one has

$$\Omega'_f - \Omega_f = \int_0^1 d\lambda\langle\hat{H}_1\rangle_\lambda \tag{24}$$

where $\langle\cdots\rangle_\lambda = \mathrm{Tr}[\cdots e^{-\beta\hat{H}(\lambda)}]/\mathrm{Tr}[e^{-\beta\hat{H}(\lambda)}]$ with $\hat{H}(\lambda) = \hat{H}_{\mathrm{BdG}} + \lambda\hat{H}_1$. The integrated function $\langle\hat{H}_1\rangle_\lambda$ are also related with the Gor'kov Green's function[23]:

$$\begin{aligned}\langle\hat{H}_1\rangle_\lambda &= 2\mathrm{Re}\{\chi_{12}[G_\lambda(1\tau,2\tau^+)_{21} + G_\lambda(2\tau,1\tau^+)_{21}]\} \\ &= 2\mathrm{Re}\{\chi_{12}T\sum_{i\omega_k}[G_\lambda(1,2;i\omega_k)_{21} + G_\lambda(2,1;i\omega_k)_{21}]\}\end{aligned} \tag{25}$$

Using Eq. (18) and (23), we have

$$G_\lambda(1,2;i\omega_k)_{21} = [G(i\omega_k)_{4\times4}(I-\lambda XA)^{-1}]_{2,3} \tag{26}$$

$$G_\lambda(2,1;i\omega_k)_{21} = [G(i\omega_k)_{4\times4}(I-\lambda XA)^{-1}]_{4,1}. \tag{27}$$

Therefore, from Eqs. (25), (26) and (27), the integration over λ in Eq. (24) is readily performed,

$$\begin{aligned}\int_0^1 (I-\lambda XA)^{-1}d\lambda &= -(XA)^{-1}\ln(I-XA) \qquad (28)\\ &= -O\begin{pmatrix} \frac{\ln(1-d_1)}{d1} & 0 & 0 & 0 \\ 0 & \frac{\ln(1-d_2)}{d_2} & 0 & 0 \\ 0 & 0 & \frac{\ln(1-d_3)}{d_3} & 0 \\ 0 & 0 & 0 & \frac{\ln(1-d_4)}{d_4}\end{pmatrix} O^{-1},\end{aligned}$$

where to treat the 4×4 matrix as an argument of logarithm function in Eq. (28), we diagonalize $XA = ODO^{-1}$ with O the transformation matrix and D the diagonal matrix with eigenvalues $d_{1,2,3,4}$.

B. Spectral function and Chebyshev polynomial approach

With the help of the local-update scheme described above, the classical phase space of Δ are sampled and thermodynamic averages of physical quantities can be obtained. As an example, we give the definition of the single-electron spectral function,

$$A(\mathbf{k},\omega) = \frac{\int D\Delta D\bar{\Delta} A_\Delta(\mathbf{k},\omega)e^{-\beta\Omega(\Delta,\bar{\Delta})}}{\int D\Delta D\bar{\Delta} e^{-\beta\Omega(\Delta,\bar{\Delta})}} \tag{29}$$

where $A_\Delta(\mathbf{k},\omega)$ denotes the single-electron spectral function for a certain configuration of Δ. $A_\Delta(\mathbf{k},\omega)$ can be derived according to

$$A_\Delta(\mathbf{k},\omega) = -\frac{1}{\pi}\mathrm{Im}\sum_{i,j} G^{\mathrm{R}}(i,j,\omega)_{11}e^{i\mathbf{k}\cdot(\mathbf{i}-\mathbf{j})}, \tag{30}$$

where the retarded Green's function is the real-space representation of the resolvent,

$$G^{\mathrm{R}}(i,j,\omega)_{11} = \langle i\uparrow|(\omega+i0^+-\hat{H}_{\mathrm{BdG}})^{-1}|j\uparrow\rangle. \tag{31}$$

Combining the above two equations, we have

$$A_\Delta(\mathbf{k},\omega) = \langle\mathbf{k}\uparrow|\delta(\omega-\hat{H}_{\mathrm{BdG}})|\mathbf{k}\uparrow\rangle, \tag{32}$$

where $|\mathbf{k}\uparrow\rangle = N^{-1/2}\sum_i e^{i\mathbf{k}\cdot\mathbf{i}}c^\dagger_{i\uparrow}|0\rangle$. Generally, one can first solve the BdG equation (11), then employ the following equation,

$$A_\Delta(\mathbf{k},\omega) = \sum_{\epsilon_n,i,j}\delta(\omega-\epsilon_n)u^i_n u^{j*}_n e^{i\mathbf{k}\cdot(\mathbf{i}-\mathbf{j})} \tag{33}$$

to calculate the spectral function for one configuration. However, since the computational effort of full diagonalization of the BdG matrix is $O(N^3)$, we will apply the Chebyshev polynomial approach[18,19], which is $O(MN)$ with $M \ll N^2$, to cut the computational cost.

We perform a Chebyshev polynomial expansion

$$\delta(x-y) = \frac{1}{\pi\sqrt{1-x^2}}\left[\mu_0 + 2\sum_{m=1}^{\infty}T_m(x)T_m(y)\right], \tag{34}$$

to handle the Dirac δ function. After substituting it into Eq (32). we have

$$A_\Delta(\mathbf{k},\omega) = \frac{\mu_0 + 2\sum_{m=1}^{M}\mu_m g_m T_m(\omega/s)}{\pi\sqrt{1-(\omega/s)^2}}, \tag{35}$$

where

$$\mu_m = \langle\mathbf{k}\uparrow|T_m(\hat{H}_{\mathrm{BdG}}/s)|\mathbf{k}\uparrow\rangle, \tag{36}$$

are Chebyshev moments. Here for numerical calculation, the infinite series in Eq. (34) has to be truncated by M as shown in Eq. (35) and to damp the consequential Gibbs oscillations the Lorentz kernel g_m is used in Eq. (35) with $g_m = \sinh[\lambda(1-m/M)]/\sinh(\lambda)$ where λ is a free parameter of the kernel and we choose $\lambda = 4$ throughout our calculation as a compromise between good resolution and sufficient damping of the Gibbs oscillations as suggested in Ref. [19]. s denotes the scaling factor ensuring the spectrum of $\hat{H}_{\mathrm{BdG}}/s$ falling into the interval $[-1,1]$, i.e. the domain of the Chebyshev polynomials.

Most computational effort is spent in the calculation of the Chebyshev moments μ_m according to Eq. (36), which reduces to sparse matrix-vector multiplications after taking advantage of the recursion relation $T_m(x) = 2xT_{m-1}(x) - T_{m-2}(x)$. Considering that the BdG Hamiltonian is sparse, the cost of matrix-vector multiplication is an $O(N)$ process and the calculation of M moments requires only $O(MN)$ computational operations. Further relations of the Chebyshev polynomials $T_{2m} = 2T_m^2 - 1$ and $T_{2m+1} = 2T_mT_{m+1} - T_1$ enable us to obtain two moments per matrix-vector multiplication. Therefore, calculation of the single-particle spectral function using the Chebyshev polynomial method is fast, efficient and direct with less memory consuming, superior to direct diagonalization [generally $O(N^3)$] of the BdG matrix.

III. NUMERICAL RESULTS

In our work, the parameters are chosen as below: $t = 1$ (as the unit of energy), $t' = -0.3$, $\mu = -0.83$, and $N =$

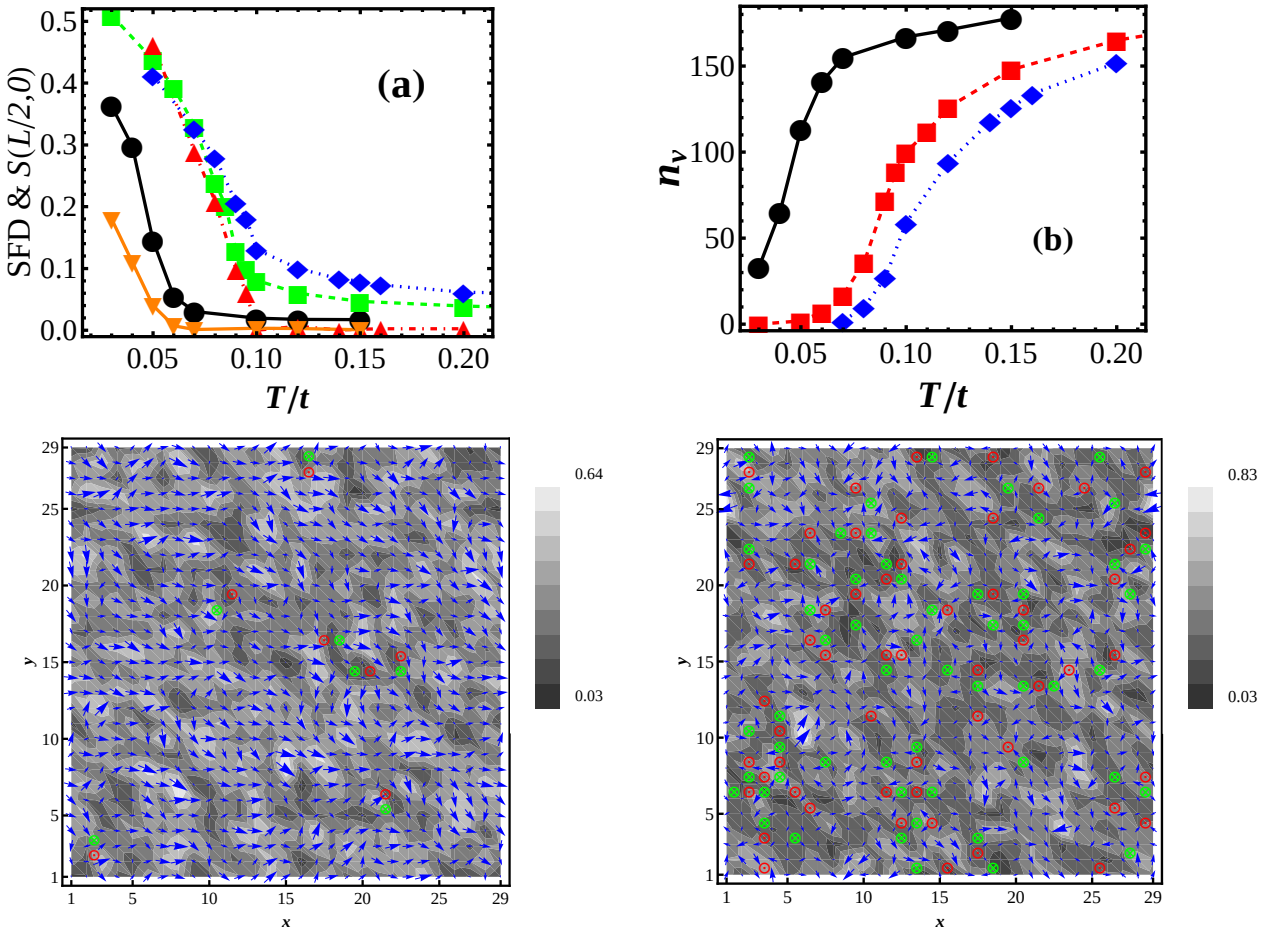


FIG. 1: Upper-left panel: Superfluid density(SFD) and the long-range phase correlation function $s(14,0)$ vs T for three different interactions. Black disks (SFD, $V=1.2$), green square (SFD, $V=2.4$), blue diamond (SFD, $V=4.0$), orange down-triangle (S(14,0), $V=1.2$), and red triangle (S(14,0), $V=4.0$). T_c is around 0.05, 0.09, 0.105 respectively. Upper-right panel: The d-wave vortex number n_v vs T for three different interactions. For each interaction, there is a region that vortices gush abruptly. Black disks($V=1.2$), red square($V=2.4$), and blue diamond($V=4.0$). Panels of the Lower row: Snap shots of the spatial distribution of the magnitude and phase of the d-wave order parameter $\Delta_d(i)$ on a 29×29 lattice (note the periodic boundary condition) at $T=0.06$ (lower left) and $T=0.12$ (lower right). The phase on each lattice site is represented by a blue arrow, while the magnitude is represented by the size of the arrow as well as the gray scale density. Also shown are the topological excitations with the red $\odot$ denoting the vortex with winding number 1 and green $\otimes$ denoting the antivortex with winding number -1.

$L\times L = 28\times 28$. According to the above parameters the average electron number is approximately 0.9 and accordingly the hole doping is 0.1. For each temperature, the first 10^3 MC sweeps are dropped to equilibrate the system. 10^3 configurations are used as samples to get statistical average. Each MC sweep includes $2N^2$ local updates to reduce the configuration correlation. By these arguments, the statistical error reduces to an acceptable level. Then, we calculate the spectral function directly with the help of the Chebyshev polynomials[19] with the truncation $M=2048$.

In Fig. 1(a), we show the superfluid density (SFD) $D_s/\pi e^2$ (see Appendix) as a function of temperature for different pairing interactions. The SFD decreases as the temperature increases and displays an apparent drop indicating a phase transition for the three interaction strengths, although SFD has a long tail above the transition temperature due to the finite size effect. By taking the leading-edge midpoint as T_c, we have $T_c \approx 0.05, 0.09, 0.105$ for $V=1.2, 2.4, 4$, respectively . Compared with the previous work[12], we find that the transition temperature increases with the interaction strength at least for $V\leq 4$. This increase of T_c with V for small to intermediate value of V is further supported if we further examine the long-range phase correlation[12] $S(L/2,0)=\frac{1}{N}\sum_{i=1}^{N} < e^{i\phi_i^{\hat{x}}} e^{-i\phi_{i+(L/2,0)}^{\hat{x}}} >$, where $\phi_i^{\hat{x}}$ denotes the phase of the pairing field $\Delta(i, i+\hat{x})$. The results are also shown in Fig. 1(a), indicating that both the SFD and $S(L/2,0)$ are measures of the phase stiffness of the condensate.

Conventionally, the phase fluctuation scenario relates the normal to SC phase transition in underdoped HTCS to the KT-type phase transition. Although people have made lots of efforts, it is still unclear how this occurs. Generally, fluctuations of the phase degrees of freedom of the superconducting order parameter can be described by the 2D XY model, the studies of which have revealed that the proliferation and unbinding of the vortex-antivortex pairs above $T_{\rm KT}$ destroys the quasi-long-range phase coherence. Here we explore this aspect by observing the vortex-type excitations in the phase field $\varphi_d(i)$ of the d-wave order parameter $\Delta_d(i) = |\Delta_d(i)|e^{i\varphi_d(i)}$. The definition of $\Delta_d(i)$ is $\Delta_d(i) \equiv [\Delta(i, i+\hat{x}) + \Delta(i, i-\hat{x}) - \Delta(i, i+\hat{y}) - \Delta(i, i-\hat{y})]/4$. The (anti)vortices are plaquette-centered topological defects of the phase field. The winding number or vorticity of the (anti)vortex is defined as the anticlockwise sum of the phase difference around each plaquette of the square lattice (divided by 2π). For each plaquette labeled by its lower-left corner i, its four vertices anticlockwisely are $i_1 = i, i_2 = i+\hat{x}, i_3 = i+\hat{x}+\hat{y}, i_4 = i+\hat{y}$. The phase difference between two NN sites for instance i_2 and i_1 is $\theta_{2,1}(i) \equiv \varphi_d(i_2) - \varphi_d(i_1) = {\rm Im}\log(\Delta_d(i_2)\Delta_d^*(i_1))$. Therefore the winding number around the plaquette i is $w(i) = [\theta_{2,1}(i) + \theta_{3,2}(i) + \theta_{4,3}(i) + \theta_{1,4}(i)]/2\pi$. $w(i) = 1$ or -1 represents a vortex- or antivortex-type topological defect around the plaquette i. The total number of (anti)vortices, i.e. n_v, which quantifies the phase fluctuation relevant to the topological excitations, is calculated according to $n_v = \sum_i \delta_{w(i),1}$, i.e. the total number of plaquettes with $w(i) = 1$ (note that without external magnetic field the antivortex number always equals to the vortex number). The temperature dependence of n_v is shown in Figs. 1(b). One can observe the abrupt jump of n_v at approximately the same temperature obtained from Fig. 1(a), giving further indication of the KT-type phase transition. For illustration, Figs. 1(c) and (d) show snapshots of the pairing fields recorded at $T = 0.06$ and $T = 0.12$ for $V = 2.4$. For these two temperatures the coherence length of the d-wave order parameter is small and the vortices can be clearly identified as shown in the figures. At the temperature well below $T_{\rm KT}$, the vortex density is dilute and all vortices are bound together as vortex-antivortex pairs as shown in Fig. 1(c). Above $T_{\rm KT}$, vortices gush and the unbinding of vortex-antivortex pair is clearly illustrated as shown in Fig. 1(d). This behavior conforms to the characteristics of KT phase transition. Together with the observation that the crossover regions of the SFD and phase correlation reduplicate that of the vortices, we can argue that the SC phase transition is of the KT type.

The single-particle excitation spectra of electrons moving in a fluctuating pairing field is highly nontrivial. Figure 2 shows the evolution of $A(k, \omega = 0)$ as a function of temperature. The momentum $\mathbf{k}$ is in the first Brillouin zone and the energy $\omega = 0$ on the Fermi level. We set the chemical potential $\mu = -0.83$ intentionally to have more discrete momenta on the underlying Fermi surface and the resulting electron number is around 0.9. At $T = 0.03$, four sharp spectral peaks right at the four gap nodes are clearly resolved in Fig. 2(a), which indicates that at temperatures well below $T_{\rm KT}$ the pair fluctuations are rather weak and the Fermi surface are actually point like as in pure d-wave superconductors. At $T = 0.09$, the height of the peaks falls while their profile extends towards the antinodal direction, i.e. the spectral weight of other $\mathbf{k}$ points along the underlying Fermi surface increases. From Figure 2, we find that this pile-up effect of spectral weight at the vicinity of the underlying Fermi surface increases with temperature, which is consistent with the ARPES observations[24,25] as well as the theoretical picture[14].

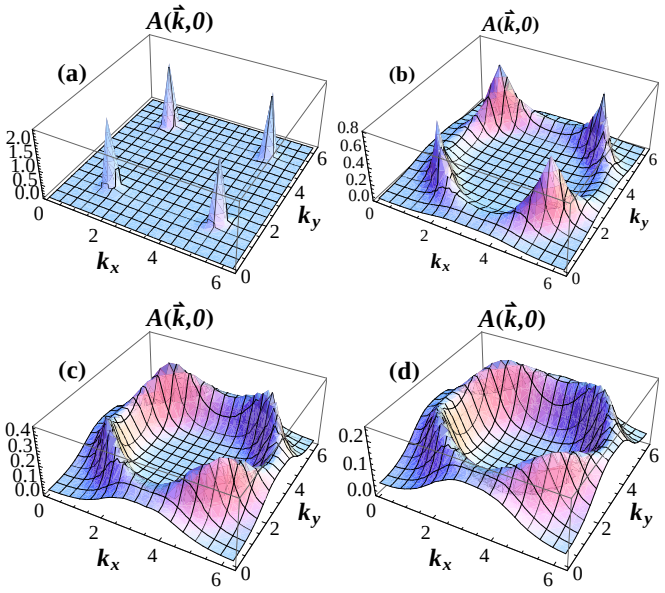


FIG. 2: Temperature dependence of the spectral function at the Fermi energy $A(\mathbf{k}, \omega = 0)$ with $\mathbf{k}$ in the first Brillouin zone ($V = 2.4$): From (a) to (d) $T = 0.03, 0.09, 0.15, 0.3$. At $T = 0.03$, four sharp spectal peaks at four nodes; With the increasing temperature, $A(\mathbf{k}, 0)$ decreases at the nodes while piles up at the other $\mathbf{k}$'s of the underlying Fermi surface; At $T = 0.3$, the spectral distribution seems like a bowl. The gap of the antinode survives at the high temperature (For 28×28 lattice, $T > 0.3$; For smaller size lattice, we find it dose not close even at $T > 0.5$).

Next, we show the energy distribution of the spectral function in Fig. 3(b) and (c) to examine the spectral gaps opened at different $\mathbf{k}$'s on the underlying Fermi surface at two different temperatures. The selected three $\mathbf{k}$'s are the node $(\frac{6\pi}{14}, \frac{6\pi}{14})$, the wave vector $(\frac{5\pi}{14}, \frac{\pi}{2})$ near the node and the antinode $(\frac{2}{14\pi}, \pi)$ as shown in Fig. 3(a). At $T = 0.05$ below the KT transition, $A(\mathbf{k}, \omega)$ for $\mathbf{k}$ at node displays a sharp peak located at zero energy. Away from the node, we find that the spectral gap opens at the selected momentum $\mathbf{k} = (\frac{5\pi}{14}, \frac{\pi}{2})$ closest to the node and increases to its largest value at the antinode, which conforms to the characteristic of d-wave superconducting gap function. At higher temperature $T = 0.09$, we find that the

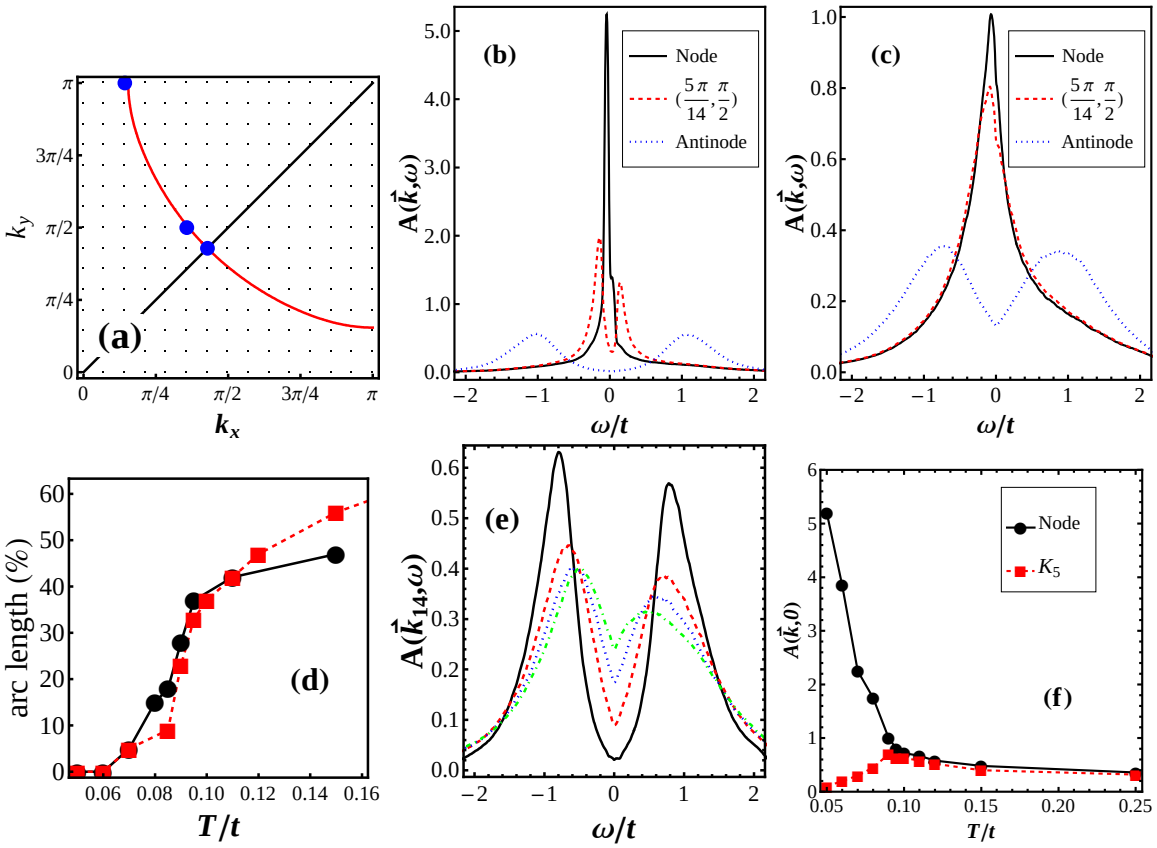


FIG. 3: (a), The Fermi surface shown as red line in the first quarter of the Brillouin zone. Three selected $\mathbf{k}$ points lying on the Fermi surface are shown as large blue dots. The spectral function $A(\mathbf{k},\omega)$ as a function of ω for this three $\mathbf{k}$ points with (b) $T = 0.05$ and (c) $T = 0.09$. (d) The Fermi-arc length versus temperature. (e) Temperature dependence of $A(\mathbf{k} = \mathbf{k}_{14},\omega)$. Black solid line($T = 0.05$), red dashed line($T = 0.08$), blue dotted line($T = 0.09$), and green dot-dashed line($T = 0.1$). (f), $A(\mathbf{k},\omega = 0)$ as a function of temperature for the node point and $\mathbf{k}_5$. For all panels $V = 2.4$.

spectral peak at the node is lowered in consistent with the observation of Fig. 2(b). Moreover the spectral gap at $\mathbf{k} = (\frac{5\pi}{14},\frac{\pi}{2})$ is closed, while a spectral peak is piled up at the zero energy, which signals the formation of the so-called Fermi arc that extends from node as far as to $\mathbf{k} = (\frac{5\pi}{14},\frac{\pi}{2})$. To quantify the length of the Fermi arc, we examine the loss of the spectral weight[24] due to the opening of the spectral gap $L = [1 - \frac{2A(\mathbf{k},\omega=0)}{A(\mathbf{k},\omega=-\Delta)+A(\mathbf{k},\omega=\Delta)}]$, where the spectral gap Δ is measured as half the peak to peak separation of the spectral function. In the ideal case $L = 1$ means the opening of a full spectral gap; while $L = 0$ identifies the closing of the gap, or in other words the formation of the Fermi arc. Here in analyzing our numerical results, we set both $L = 0.1$ and $L = 0.15$ as the threshold for the arc formation. The results are plotted in Fig. 3(d) where the variation of the length of Fermi arcs as a function of temperature is shown. For both parameters, the arc length exhibits apparent rise near T_c, which is consistent with the APRES measurement[25]. In addition, this jump locates around the same temperature where SFD, phase correlation, and the vortex density changes most remarkably, indicating the importance of pair fluctuation in the formation of the Fermi arc. We cut the underlying Fermi surface between the node and antinode in the first quarter of the first Brillouin zone into 20 equally spaced parts, with $\mathbf{k}_0$ denoting the node and $\mathbf{k}_{20}$ the antinode. We examine the $\mathbf{k}_{14}$ point in Fig. 3(e). It is clearly shown that there is a continuous increase of the spectral weight at the Fermi level from $T = 0.05$ to $T = 0.1$, while the spectral gap shrinks as the temperature increases, which can be explained by the increasing broadening effect due to the thermal pairing fluctuation.

Now we report the second shift of the zero energy spectral weight. According to Figs. 3(b) and (c), we notice that the zero energy spectral weight at the node/antinode is always decreaing/increasing with temperature. However for the $\mathbf{k}$ points near the node, the zero energy spectral weight first increases with temperature and then decreases above a temperature whose value depends on $\mathbf{k}$ as shown in Fig. 3(f). We call this phenomenon the second shift, which can be understood according to the theory of Berg and Altman[14]. Because of the Doppler-shift effect, the zero-energy spectral weight of the node is transferred to its neighboring $\mathbf{k}$ points and is gradually exhausted nearby T_c; the neighboring points received the zero energy spectral weight from the node, and also

due to the same effect, shift their zero-energy spectral weight to their neighboring points. The higher the temperature is, the less they get and the more they shift. For high enough temperature, both the node and the neighboring points have approximately equal amount of the zero-energy spectral weight as shown in figure 3(f), and the zero-energy spectral weights of these points saturate and begin to decrease.

IV. CONCLUSIONS

In conclusion, we have carried out the classical Monte Carlo simulation of the 2D attractive Hubbard model. We have presented a local-update procedure based on the Matsubara Green's Function using Nambu-Gor'kov formalism, which speeds up the exploring of the configuration space. We found that thermal fluctuations do contribution to the pile up of low-energy spectral weight on the underlying Fermi surface and the evolution of fermi arcs with temperature. The abrupt jump of the arc length is a qualitative result caused by the continuous piling up of zero energy spectral weight, and the second shift suggests that E. Berg and E. Altman's idea works better than simply thermally broadening effect. Finally, taking superfluid density as the SC criteria is effective when interaction V is small.

The work was supported by the Natural Science Foundation of China No.10674179.

V. APPENDIX: SUPERFLUID DENSITY

The superfluid density can be obtained applying the linear response theory to the homogenous superconducting state[26]. Here we will use Gor'kov Green's function to express the superfluid weight. We start from the following formula [26]

$$\frac{D_s}{\pi e^2} = \frac{1}{N\hbar^2}\langle -\hat{K}_x\rangle - \Pi_{xx}(q_x = 0, q_y \to 0, i\Omega_m = 0), \tag{37}$$

where D_s represents the superfluid weight and measures the ratio of superfluid density to mass. Here $\hat{K}_x$ denotes the electron kinetic energy along x direction and

$$\langle -\hat{K}_x\rangle = \sum_{\mathbf{k}\sigma}\frac{\langle c^\dagger_{\mathbf{k}\sigma}c_{\mathbf{k}\sigma}\rangle}{m^x_{\mathbf{k}}} = 2\sum_{\mathbf{k},\omega_n}\frac{G_{11}(\mathbf{k}, i\omega_n)e^{i\omega_n 0^+}}{m^x_{\mathbf{k}}}, \tag{38}$$

$m^x_{\mathbf{k}} = (\partial^2\varepsilon_{\mathbf{k}}/\partial k_x^2)^{-1}$ the electron effective mass with $\varepsilon_{\mathbf{k}} = -2t(\cos k_x + \cos k_y) - 4t'\cos k_x \cos k_y$ the electron dispersion. Π_{xx} is the current-current correlation function defined in momentum and imaginary-time space

$$\Pi_{xx}(\mathbf{q}, \tau) = \frac{1}{N}\langle \mathrm{T}_\tau \hat{j}_x(\mathbf{q}, \tau)\hat{j}_x(-\mathbf{q}, 0)\rangle, \tag{39}$$

where $\hat{j}_x(\mathbf{q}) = \frac{1}{\hbar}e^{iq_x/2}\sum_{\mathbf{k}\sigma} v^x_{\mathbf{k}+\mathbf{q}/\mathbf{2}}c^\dagger_{\mathbf{k}\sigma}c_{\mathbf{k}+\mathbf{q}\sigma}$ the current-density operator, and $v^x_{\mathbf{k}} = \partial\varepsilon_{\mathbf{k}}/\partial k_x$ denotes the group velocity of electron. Performing Fourier transform with respect to imaginary time, we have

$$\Pi_{xx}(\mathbf{q}, i\Omega_m) = \int_0^\beta d\tau e^{i\Omega_m\tau}\Pi_{xx}(\mathbf{q}, \tau), \tag{40}$$

Combining Eq. (37), (38) and (40) followed by straightforward derivation, we have the equation for superfluid density expressed using the Gor'kov Green's function,

$$\frac{n_s}{m^*} \equiv \frac{D_s}{\pi e^2} = \frac{2}{N\hbar^2}\sum_{\mathbf{k},\omega_n}\frac{G_{11}(\mathbf{k}, i\omega_n)e^{i\omega_n 0^+}}{m^x_{\mathbf{k}}} + \frac{1}{N\hbar^2\beta}\sum_{\mathbf{k},\omega_n}\left(v^x_{\mathbf{k}+\mathbf{q}/\mathbf{2}}\right)^2 \mathrm{tr}[G(\mathbf{k}, i\omega_n)G(\mathbf{k}+\mathbf{q}, i\omega_n)]\Big|_{q_x=0, q_y\to 0}. \tag{41}$$

Then we will use the above formula to pair-fluctuating superconductors, whose superfluid weight is given by

$$D_s = \frac{\int D\Delta D\bar{\Delta} e^{-\beta\Omega(\Delta,\bar{\Delta})}D_s(\Delta, \bar{\Delta})}{\int D\Delta D\bar{\Delta} e^{-\beta\Omega(\Delta,\bar{\Delta})}}, \tag{42}$$

where, $D_s(\Delta, \bar{\Delta})$ denotes the superfluid weight for a certain configuration Δ. Considering that Δ is spatially inhomogeneous, we should first perform Fourier transform on the real-space Gor'kov Green's function which has been obtained and updated during the random walk through the configuration space,

$$G(\mathbf{k}, i\omega_n; \Delta) = \frac{1}{N}\sum_{i,j} G(i, j, i\omega_n; \Delta)e^{i\mathbf{k}\cdot(\mathbf{i}-\mathbf{j})}. \tag{43}$$

After the transformation, Eq. (43) is inserted into Eq. (41) to calculate the superfluid density corresponding to one configuration and then using Eq. (42) to obtain the statistical average over configurations.

[1] H. Ding, *et al.*, Nature **382**, 51-54 (1996).

[2] D.S. Marshall, *et al.*, Phys. Rev. Lett. **76**, 4841 (1996).

[3] A. G. Loeseret, *et al.*, Science **273**, 325 (1996).
[4] M. R. Norman, *et al.*, Nature **382**, 157-160 (1998).
[5] A. M. S. Tremblay, *et al.*, Low Temp. Phys. **32**, 424 (2006).
[6] E. Z. Kuchinski, *et al.*, J. Exp. Theor. Phys. **103**, 415 (2006).
[7] C. Li, S. Zhou, Z. Wang, Phys. Rev. B **73**, 060501 (2006).
[8] V. J. Emery, *et al.*, Nature **374**, 434-437 (1995).
[9] M. Randeria, N. Trivedi, A. Moreo and R. T. Scalettar, Phys. Rev. Lett. **69**, 2001 (1992).
[10] M. Randeria *et al.*, In Proceedings of the International School of Physics Enrico Fermi Course CXXXVI on High Temperature Superconductors(53 IOS Press, 1998).
[11] T. Eckl, D. J. Scalapino, E. Arrigoni, and W. Hanke, Phys. Rev. B **66**, 140510(R) (2002).
[12] M. Mayr and G. Alvarez and C. Şen and E. Dagotto, Phys. Rev. Lett. **94**, 217001 (2005).
[13] M. Franz and A. J. Millis, Phys. Rev. B. **58**, 14572 (1998).
[14] E. Berg and E. Altman, Phys. Rev. Lett. **99**, 247001 (2007).
[15] G. Alvarez and E. Dagotto, Phys. Rev. Lett. **101**, 177001 (2008).
[16] M. Khodas and A. M. Tsvelik, Phys. Rev. B, **81**, 094514 (2010).
[17] T. Li and Q. Han, J. Phys.: Condens. Matter **23**, 105603 (2011); arXiv:1003.1783v1 (2010).
[18] Q. Han, T. Li and Z. D. Wang, Phys. Rev. B **82**, 052503 (2010); arXiv:1005.5497v1 (2010).
[19] A. Weiβe, *et al*, Rev. Mod. Phys. **78**, 275-306 (2006).
[20] A. Erez and Y. Meir, Europhys. Lett. **91**, 47003 (2010).
[21] Naoto Nagaosa, *Quantum Field Theory in condensed Matter Physics*, (Springer-Verlag Berlin Heidelberg, 1999).
[22] Y. Dubi, *et al.*, Nature **449**, 876-888 (2007).
[23] J. W. Negele, and H. Orland, *Quantum Many-Particle Systems*, (Westview Press, Boulder, 1998).
[24] A. Kanigel, *et al.*, Nature Phys. **2**, 447-451 (2006).
[25] A. Kanigel, *et al.*, Phys. Rev. Lett. **99**, 157001 (2007).
[26] D. J. Scalapino, S. R. White, and S. C. Zhang, Phys. Rev. Lett. **68**, 2830 (1992).